J. Fluid Mech. (2015), *vol.* 765, R2, doi:10.1017/jfm.2015.1

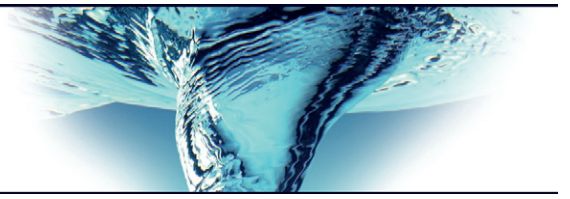

JFM RAPIDS
journals.cambridge.org/rapids

Flexibility increases lift for passive fluttering wings

Daniel Tam†

Laboratory for Aero- and Hydrodynamics, Technische Universiteit Delft, Delft, The Netherlands

(Received 22 August 2014; revised 4 December 2014; accepted 24 December 2014;
first published online 16 January 2015)

We examine experimentally the influence of flexibility on the side-to-side fluttering motion of passive wings settling under the influence of gravity. Our results demonstrate the existence of an optimal flexibility that allows flexible wings to remain airborne twice as long as their rigid counterparts of identical mass and size. Flow visualization and measurements allow us to elucidate the role of flexibility in generating increased lift and wing circulation by shedding additional vorticity at the turning point. Theoretical scalings are derived from a reduced model of the flight dynamics and yield quantitative agreement with experiments. These scalings rationalize the strong positive correlation between flexibility and flight time. Our experimental results and theoretical scalings represent an ideal system for the validation of computational approaches to model biologically inspired fluid–structure interaction problems.

Key words: aerodynamics, flow–structure interactions, swimming/flying

1. Introduction

The aerial display of flying insects has long captivated biologists and physicists alike and is a source of inspiration for the design of lightweight flapping micro-air vehicles (MAVs) (Percin *et al.* 2011). To remain in the air, the flapping motion of insect wings generates much higher lift forces than predicted by classical aerodynamic theory. The importance of unsteady aerodynamics has been discussed in previous work, and the crucial role of vortices, such as stable leading-edge vortices, has been identified (Birch & Dickinson 2001). Both insects and MAVs are required to be lightweight and their wings are hence often flexible (Combes & Daniel 2003; Percin *et al.* 2011). The flow-induced elastic deformation of flat flexible structures represents a rich class of fundamental problems in the field of fluid–body interactions. Recently, two problems have received considerable attention: the flapping flag instability (Shelley, Vandenberghe & Zhang 2005; Eloy *et al.* 2008) and the flow-induced reconfiguration of flexible bodies (Alben, Shelley & Zhang 2002). These studies have

† Email address for correspondence: d.s.w.tam@tudelft.nl

highlighted the crucial role of flexibility in drag reduction (Alben *et al.* 2002) and optimal thrust generation (Heathcote & Gursul 2007; Spagnolie *et al.* 2010). Previous studies have suggested flexibility to improve locomotion through resonant mechanisms (Michelin & Llewellyn-Smith 2009; Masoud & Alexander 2010). However, the relevance of resonance to flapping flight has been recently questioned (Ramananarivo, Godoy-Diana & Thiria 2011).

The present study focuses on a less explored question relevant to the design of light MAVs and valuable for the understanding of biological locomotion: the influence of flexibility on vortex generation and aerodynamic lift. We here present the results of an experimental study of passive flexible wings undergoing an unsteady fluttering motion. The motion of free bodies settling or rising in a surrounding fluid under the influence of gravity has generated a high level of interest (Huang *et al.* 2013; Heisinger, Newton & Kanso 2014; Hu & Wang 2014; Tchoufag, Fabre & Magnaudet 2014). Recent work on freely falling flat plates has focused on rigid wings (Mahadevan 1996). Such uniformly loaded plates are longitudinally unstable, which prevents them from gliding steadily and gives rise to an unsteady motion. Most of the previous work on falling plates has examined the transition from a side-to-side fluttering motion to a tumbling motion (Belmonte, Eisenberg & Moses 1998; Andersen, Pesavento & Wang 2005), whereby the wing undergoes full rotations. The present work examines the effect of flexibility on passive flight. We investigate whether passive elastic deformations can increase lift and allow the wings to remain airborne for longer time periods. In the tumbling regime, flexible wings induce less lift than rigid wings and reduce the flight time (Tam *et al.* 2010). Here, we focus on the fluttering regime.

Our experiments reveal a dramatic increase of lift and flight time due to subtle chordwise dynamic wing deformations, in sharp contrast to previous steady-state studies reporting a decrease in lift due to chordwise flexibility (Zhao *et al.* 2010). The extent of the lift increase is rationalized by deriving scaling laws for the flight characteristics. We identify a non-resonant lift increase mechanism that allows flexible wings to shed stronger vortices leading to increased circulation and lift on the wings.

2. Experimental approach

For experimental ease, our study is conducted in a water tank 140 cm tall, 100 cm wide and 10.5 cm deep (figure 1*a*). Our wings correspond to flat rectangular plates of chord length l, thickness h and span length L and are released at the top of the tank and freely settle through water of density ρ under the influence of gravity $\boldsymbol{g}$, see figure 1(*a*). Wings are characterized by their density ρ_s and bending rigidity in the chordwise direction κ. In order to both settle to the bottom of the tank and elastically deform, the wings are required to be both negatively buoyant and flexible. Consequently, we manufacture wings from two different materials. We use metallic brass of density 8500 kg m^{-3} to allow the wings to settle in water as well as the elastic polymer vinylpolysiloxane of density 1050 kg m^{-3} to allow the wings to be compliant. The wings are assembled by arranging equally spaced brass bars in a custom-made mould before casting the elastic polymer (figure 1*a*). The spanwise dimension of the wings, $L = 10$ cm, closely coincides with the depth of the tank in order to constrain the experiment to be two dimensional. Millimetre-sized polished stainless steel beads are fixed at the four corners of the wing, allowing the wing to freely move in water with negligible friction against the glass wall of the tank.

The dynamics of the passive wings is characterized by two non-dimensional numbers,

$$I^\star = \frac{\rho_s h}{\rho l} \quad \text{and} \quad C_y = \frac{\rho U^2 l^3}{\kappa}, \tag{2.1a,b}$$

where $U = \sqrt{(\rho_s - \rho)hg/\rho}$ is the characteristic settling velocity deduced from a force balance between weight and buoyancy on the one hand and hydrodynamics on the other. Here, $I^\star$ is the non-dimensional moment of inertia, which can also be interpreted as the inverse of the added mass parameter. In our study, the material densities are not varied and $I^\star$ is a geometric parameter characterizing the cross-sectional aspect ratio h/l of the wings. The non-dimensional number C_y is the Cauchy number, which corresponds to the ratio of hydrodynamic to elastic bending forces and increases with the flexibility of the wing. In all experiments, the Reynolds number is of the order of $Re \approx 10^5$ and does not vary significantly between experiments. In this study, the influences of $I^\star$ and C_y were investigated by varying the cross-sectional geometry of the wing and the Young's modulus of the elastic polymer independently. We considered five wing cross-sectional geometries, $I^\star = 0.05$, 0.07, 0.10, 0.17, 0.24, by varying the thickness of the brass bars ($h = 0.4$–1.6 mm) and the chord length of the wings ($l = 41$–80 mm). All five cross-sectional geometries have low thickness to chord aspect ratio, $h/l = 0.005$–0.039, and the wings can be considered to be thin flat plates. All of these wings undergo a fluttering motion in agreement with previous experimental studies, which have determined the transition to tumbling motion to occur beyond a critical value of the non-dimensional moment of inertia of $I^\star_{crit} \approx 0.4$ (Belmonte *et al.* 1998). Using nine different elastic polymers with Young's moduli ranging from $E = 0.26$ to 1.2 MPa, the bending rigidity in the chordwise direction κ is varied. The natural frequencies of the flexible wings are no less than 10 Hz. Fully rigid wings are also considered by fixing thin mylar films to the upper and lower surfaces of the wings. The Cauchy number ranges between 0 for rigid wings and 70 for the most flexible ones. The range of Reynolds and Cauchy numbers investigated in our experiments is relevant to many problems of objects, paper, leaves and seedpods falling in air.

Wings are released in the water tank and their descent is recorded using high-speed imaging at 150–250 f.p.s. Figure 1(*b*) represents successive snapshots recorded with our experimental set-up. The videos are processed to extract the two-dimensional trajectory of the wing $\boldsymbol{X}(t) = (x(t), y(t))$, the wing velocity $U(t) = (v_x(t), v_y(t))$ and the pitch angle $\theta(t)$ between the horizontal $\hat{x}$ and chord $\hat{x}'$ directions, figure 1(*a*). The side-to-side fluttering motion is characterized by turning points, where the wings stop and change direction, separated by gliding intervals, where the wings descend due to gravity. Characteristic quantities are deduced from the analysis of the trajectories: the horizontal Δx and the vertical Δy distances between consecutive turning points, the frequency of the oscillatory motion f, the average vertical descent velocity of the wing U_d and the characteristic flight time $\tau_f = l/U_d$ required to descend over one chord length l at the average descent rate U_d (figure 1*b*). Wing shape is characterized by the deflection, which corresponds to the distance from a point along the deformed camberline to the straight chordline joining the leading and trailing edges. The extent of elastic deformation is recorded by measuring the maximum deflection along the wing δ. In addition, the two-dimensional flow velocity field $\boldsymbol{u}$ in the tank is measured in separate sets of experiments using double frame particle image velocimetry (PIV). Figure 1(*c*) represents the typical vorticity field left behind a fluttering wing. All experimental data are non-dimensionalized with the characteristic velocity as a reference velocity $U_{ref} = U$, the dimension of the chord as a reference length $l_{ref} = l$ and the reference time scale $t_{ref} = l/U$. Henceforth, all variables are non-dimensional unless otherwise specified.

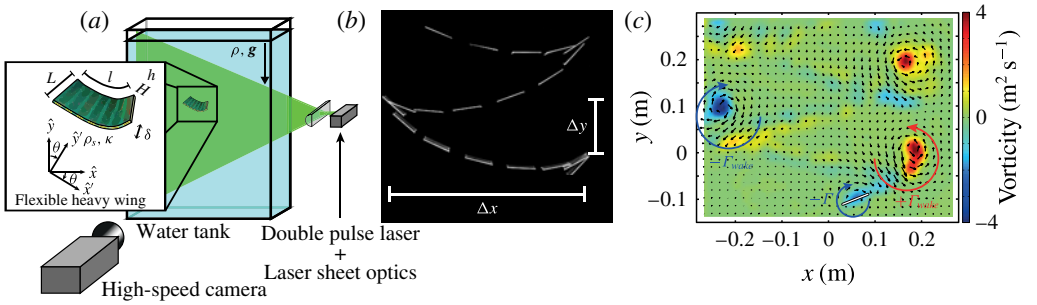

FIGURE 1. (*a*) Experimental set-up. (*b*) Superimposed snapshots of the fluttering motion ($C_y = 0$ and $I^\star = 0.1$). Time between snapshots: 125 ms. (*c*) Particle image velocimetry measurements of the vorticity and velocity fields ($C_y = 10$ and $I^\star = 0.1$). The wing is represented by a line and the wing circulation Γ and wake vortices Γ_{wake} are highlighted by coloured arrows.

3. Experimental results

We proceed by detailing our experimental observations. For each cross-sectional geometry characterized by $I^\star$, the effect of flexibility is isolated by studying wings with increasing Cauchy number from values corresponding to rigid wings, $C_y = 0$, to highly flexible wings, $C_y \approx 70$. Following their release, the wings settle in a stable periodic two-dimensional left-to-right fluttering motion (see the supplementary movies available at http://dx.doi.org/10.1017/jfm.2015.1). The fluttering motion is always observed for all but the most flexible wings. For very flexible wings ($C_y \geqslant 60$), the stability of the fluttering motion is lost to an unstable flapping motion (Shelley *et al.* 2005), resulting in rapid descent, see the supplementary movies. The flexibility at which this transition occurs is in agreement with previous experimental work (Shelley *et al.* 2005). We henceforth restrict our attention to the stable fluttering motion, which is the only dynamics observed for $C_y \leqslant 60$.

Flexible wings deform during the fluttering motion. Typical wing shapes are reproduced in figure 2(*a*). Rigid wings, $C_y = 0$, remain flat throughout their descent, while flexible wings exhibit small upward bending deformation δ, generally not exceeding 5 % of the chord length l. Figure 2(*c*) represents the time variations of the deformation δ during the fluttering motion for $I^\star = 0.1$ and $C_y = 15$. During gliding intervals, the deformation does not exceed 1 % and the wings can be considered to remain flat. Elastic deformations are restricted to short time periods at the turning points, where δ reaches a maximal value $\bar{\delta}$ of the order of 4 %, see figure 2(*c*). In our experiments, the chord length does not exceed 8 cm and the dimensional deflection does not exceed 5 mm. In figure 2(*a*), the white arrows indicate the frames in the sequence of snapshots, when the maximal deformation $\bar{\delta}$ is observed. The wing deformations $\bar{\delta}$ remain very small for all wings, as can also be seen in the supplementary movies. Figure 2(*d*) represents the maximal wing deformation $\bar{\delta}$ recorded at the turning points for wings of increasing flexibility. The elastic deformation $\bar{\delta}$ is found to increase linearly with the flexibility of the wing C_y.

While the extent of elastic deformation remains small, its effect on the flight characteristics is striking. For each value of $I^\star$, the fluttering amplitudes Δx and Δy decrease severalfold as C_y is increased, see figure 3(*a,b*). Concurrently, the frequency f of the fluttering motion increases severalfold, see figure 3(*c*). The characteristic flight

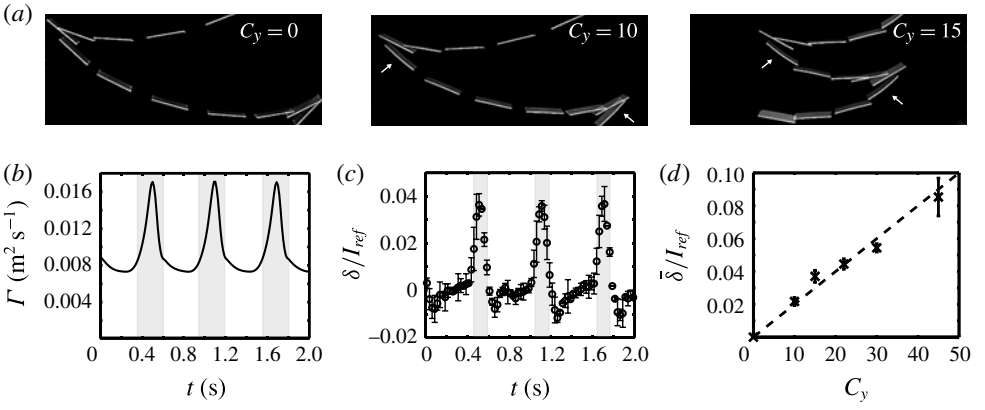

FIGURE 2. (*a*) Superimposed snapshots of the fluttering motion for $I^\star = 0.1$ and increasing C_y. White arrows highlight wing shapes, when the deformation δ reaches its maximum value $\bar{\delta}$. (*b*) Circulation measurements deduced from high-speed imaging as a function of time for a fluttering wing ($I^\star = 0.1$ and $C_y = 15$) (*c*). Bending deformation δ as a function of time for the same fluttering wing as in (*b*). (*d*) Maximum bending deformation $\bar{\delta}$ measured at the turning point as a function of the Cauchy number C_y for fluttering wings ($I^\star = 0.1$).

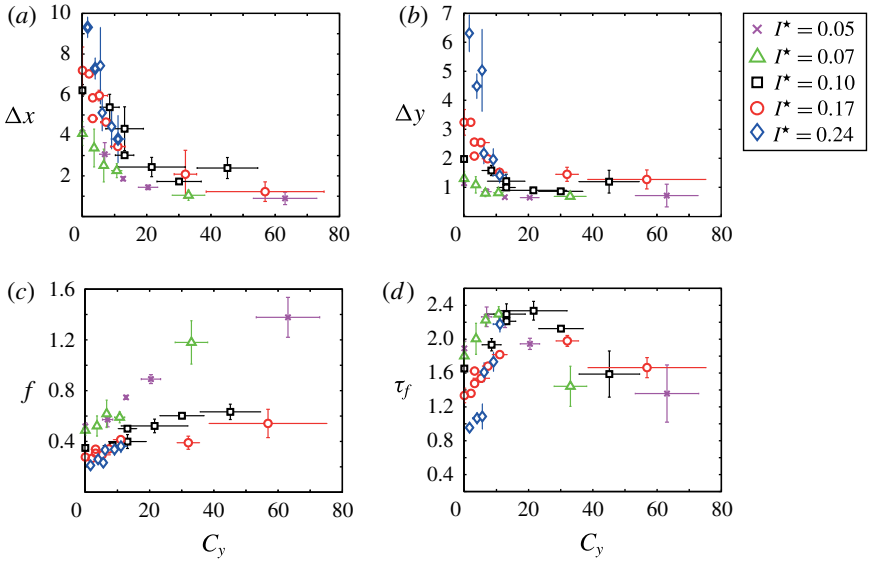

FIGURE 3. Influence of wing flexibility on flight characteristics. For each $I^\star$, the wing flexibility C_y is varied and the dependence of the flight characteristics with respect to the Cauchy number C_y is recorded. The panels correspond to (*a*) Δx, the horizontal amplitude of the fluttering motion, (*b*) Δy, the vertical amplitude of the fluttering motion, (*c*) f, the frequency of the fluttering motion, (*d*) τ_f, the characteristic flight time. All quantities are non-dimensional.

time τ_f is the most relevant quantity in our study as it characterizes how long the wing remains airborne. The non-dimensional flight time τ_f is precisely the inverse of the non-dimensional average descent velocity U_d. The flight time τ_f strongly depends on the wing flexibility C_y (figure 3*d*). For each wing geometry $I^\star$, τ_f increases from its value for rigid wings at $C_y = 0$ to a maximum at some optimal flexibility $C_y^\star$. For $C_y \geqslant C_y^\star$, τ_f decreases with increasing C_y (figure 3*d*). For $I^\star = 0.05$, the flight time of wings of optimal flexibility is 1.22 times longer than for rigid wings. This increased flight time is enhanced at higher $I^\star$ values. For the highest value, $I^\star = 0.24$, the optimally flexible wing remains aloft 2.5 times longer than its rigid counterpart, corresponding to a more than twofold increase in flight time. While the fluttering frequency does increase with flexibility, the dimensional values of f remain of the order of 1 Hz, which is one order of magnitude lower than the natural frequencies of the wings. The optimal flight time due to flexibility is hence not caused by a resonant mechanism. The effect of flexibility on the flight characteristics is best observed by watching recorded videos of fluttering wings of identical geometry and increasing flexibility provided in the supplementary material.

Velocity and vorticity fields obtained from PIV measurements provide key insight into the fluttering dynamics and shed light on the mechanisms generating wing circulation. Figure 1(*c*) represents the typical vorticity field produced by a descending wing. Particle image velocimetry measurements were performed for wings of varying geometry $I^\star$ and flexibility C_y. Two key vortical elements can be identified in the vorticity distribution. First, the bound vorticity on the wing corresponds to the wing circulation at the origin of the Joukowski lift. Second, vortices are shed at each turning point: a strong vortex and an associated much weaker counter-rotating one (see figure 1*c*). Outside of these two vortical elements, little vorticity is present in the flow. This characteristic vortex distribution is observed for all fluttering wings of varying C_y and $I^\star$. We estimate the wing circulation during the gliding interval Γ and the circulation around the asymmetric vortex pair shed at the turning point Γ_{wake}. We do so by evaluating the line integral $\Gamma = \oint_{\mathscr{C}} \boldsymbol{u} \cdot \mathrm{d}\boldsymbol{l}$, where $\mathscr{C}$ represents a closed contour closely following the vortical element of interest and $\boldsymbol{u}$ is the flow velocity interpolated on $\mathscr{C}$. In addition, the wing circulation Γ was also measured from the high-speed imaging experiments. The acceleration of the wing is computed from the recorded time-resolved wing trajectory $\boldsymbol{X}(t) = (x(t), y(t))$. One can directly deduce the total aerodynamic force acting on the wing. Assuming a Joukowski lift $\rho\Gamma|\boldsymbol{U}|$ (Andersen *et al.* 2005), one can estimate the wing circulation from the lift force. Figure 2(*b*) represents the time variations of the circulation deduced from high-speed imaging for $I^\star = 0.1$ and $C_y = 15$. During gliding intervals, the circulation remains relatively constant at a value of 0.008 $\mathrm{m}^2\ \mathrm{s}^{-1}$. Turning points correspond to the shaded areas, for which the estimate is not expected to be accurate as the wing velocity $\boldsymbol{U}$ vanishes. The wing circulation was estimated separately using PIV and high-speed imaging and the measurements were in perfect agreement and confirmed the accuracy of the PIV measurements. For a given cross-sectional geometry $I^\star$, we observe flexible wings to develop larger wing circulation Γ than their rigid counterparts and to shed stronger vortices Γ_{wake} at the turning points (see figure 4). The increase in wing circulation due to flexibility is significant. For $I^\star = 0.24$ and $C_y = 11$, the circulation is 2.1 times larger than for the corresponding rigid wing. The circulation increases deduced from the PIV measurements and from high-speed imaging are in agreement.

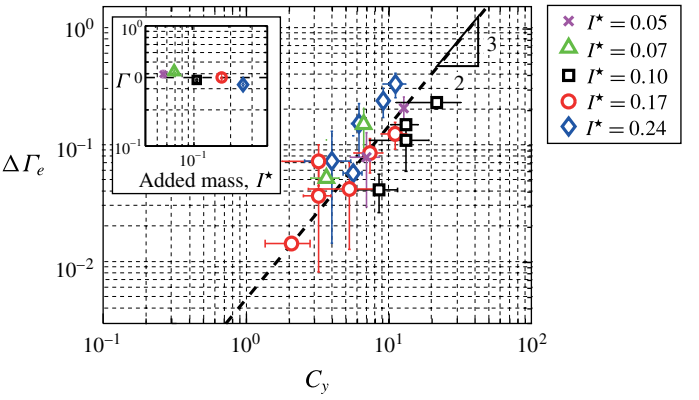

FIGURE 4. Dependence of $\Delta\Gamma_e = \Gamma - \Gamma_0$ on wing flexibility C_y. Each data set corresponds to a fixed cross-sectional geometry with $0.05 \leqslant I^\star \leqslant 0.24$. Inset: the circulation for rigid wings ($C_y = 0$) is independent of wing geometry $I^\star$.

4. Theoretical scalings

In the following, we elucidate the physical mechanisms responsible for the increase in lift and flight time. Hence, we focus exclusively on flexibilities between the rigid limit $C_y = 0$ and the optimal value $C_y^\star$, for which the flight time is maximum. In this discussion, we consider a simplified vorticity distribution as follows. The bound vorticity on the wing is reduced to a single point vortex Γ attached to the wing and each asymmetric vortex pair is represented by a point vortex at the turning point, whose circulation Γ_{wake} corresponds to the circulation around the vortex pair (figure 1*c*). Outside of these vortices, we assume the flow to be irrotational in agreement with our PIV data. This simplified vorticity distribution is characteristic of the observed distribution for all fluttering wings.

During a gliding interval, the wing descends from one turning point to the following one under the influence of gravity with a circulation of $+\Gamma$. At the turning point, the wing comes to rest and sheds a wake vortex $+\Gamma_{wake}$ before resuming flight in the opposite direction with a circulation $-\Gamma$. In this simplified vorticity field, Kelvin's circulation theorem has two important consequences: (i) Γ and Γ_{wake} remain constant in time and (ii) $\Gamma_{wake} = 2\Gamma$. This equality follows directly from the conservation of circulation for a contour around a turning point, considering that the circulation of the wing is initially $+\Gamma$ and becomes $-\Gamma$ after the wake vortex Γ_{wake} is shed. This problem is not without correspondence with classical starting vortices. These two inferences are verified experimentally from the measurements of circulation around the wing and around wake vortices from each PIV data set. For each value of $I^\star$, Γ varied by no more than 8 % during the gliding interval and the ratio of wake to wing circulation was $\Gamma_{wake}/\Gamma = 2.01 \pm 0.08$. We conclude that the wing circulation Γ is created predominantly at the turning points and remains relatively constant through the subsequent gliding interval.

The following physical picture emerges. Wing flexibility acts at the turning points, where elastic deformations occur. These passive deformations allow flexible wings to shed stronger wake vortices and to generate larger wing circulation than their rigid counterparts of equal $I^\star$. During gliding intervals, both rigid and flexible wings experience lift forces, which depend on the wing circulation created at the turning

point. We proceed by deriving theoretical scalings to rationalize the effect of flexibility on fluttering wings.

4.1. *Scaling for the wing circulation*

Generally, circulation is created when wings with sharp edges are accelerated and vorticity is shed at the trailing edge. There is an analogy between the wake vortices in our experiment and classical starting vortices. At the turning point, the wing is first accelerated by gravity and fluid flows around the leading and trailing edges. Vorticity develops at the two wing tips and the pressure distribution corresponding to this vorticity distribution creates a bending moment responsible for the brief upwards bending deflection δ observed (see figure 2*c*). Thereafter, the vorticity at the trailing edge is shed to satisfy the Kutta condition, cancelling the bending moment, and the trailing edge is further accelerated by elastic forces until the wing returns to a flat configuration. This description agrees with the earlier observation that deformations arise only at the turning points.

Two forces thus contribute to the acceleration experienced by the wing tips: gravity and wing elasticity. Accordingly, the wing circulation is written as the sum of two terms, $\Gamma = \Gamma_0 + \Delta\Gamma_e$, where Γ_0 is the circulation due to the gravitational acceleration of the equivalent rigid wing and $\Delta\Gamma_e$ characterizes the contribution of elasticity. Circulation scales as the product of a characteristic length times a characteristic velocity. Theoretical scalings for each contribution Γ_0 and $\Delta\Gamma_e$ can be derived. Gravity accelerates the wing downwards from rest to a descent velocity, which scales with the characteristic settling speed U. The dimensional circulation due to gravity is hence expected to scale with $\Gamma_0 \sim lU$, which in non-dimensional terms translates to a constant Γ_0 independent of $I^\star$ and C_y. This scaling is validated experimentally by measuring the circulation around rigid wings, $\Gamma(C_y = 0) = \Gamma_0$, for which the contribution of elasticity vanishes. The circulation Γ_0 is constant and independent of $I^\star$ in agreement with the scaling (see inset in figure 4). Next, we consider the additional $\Delta\Gamma_e$ generated when the bending energy due to the deformation δ is released. In this case, the relevant length scale is the maximal deformation at the turning point $\bar{\delta}$ and the relevant velocity scale is the velocity of the wing tip $\bar{\delta}/\tau$ due to elastic forces, where τ is the characteristic time of the elastic response. The following scaling for the dimensional circulation can be deduced: $\Delta\Gamma_e \sim \bar{\delta}(\bar{\delta}/\tau)$. The non-dimensional deflection scales linearly with the Cauchy number, $\bar{\delta}/l \sim C_y$, in agreement with our experimental observations of δ (see figure 2*d*). The non-dimensional time of the elastic response scales with $\tau/t_{ref} \sim C_y^{1/2}$. Together, these scalings yield for the non-dimensional circulation

$$\Delta\Gamma_e \sim C_y^{3/2}. \tag{4.1}$$

The 3/2 exponent of this nonlinear scaling implies that wing circulation and wake vortices greatly increase with flexibility. This result is verified against our experimental measurements of Γ for wings of varying flexibility C_y. For each different wing geometry $I^\star$, we consider the experimental data recorded for wings, for which we observed an increase in flight time. These wings are characterized by a Cauchy number ranging from the rigid limit $C_y = 0$ to the value at which the maximal flight time was recorded $C_y = C_y^\star$. For all flexible wings, $\Delta\Gamma_e$ is estimated experimentally as $\Delta\Gamma_e = \Gamma - \Gamma_0$, where Γ is the circulation measured around the flexible wing and Γ_0 is the circulation measured around its rigid counterpart of identical geometry. For each separate wing geometry $I^\star$, this 3/2 exponent is verified experimentally by

plotting $\Delta\Gamma_e(C_y)$ on a 'log–log' scale, see figure 4. At the optimal $C_y^\star$, $\Delta\Gamma_e$ is of the same order of magnitude as Γ_0 and the increase in wing circulation due to flexibility is significant.

4.2. *Scalings for the flight characteristics*

We now turn to the gliding intervals and quantify the effect of increased circulation on the flight characteristics. Previous studies (Mahadevan 1996; Belmonte *et al.* 1998; Andersen *et al.* 2005) have investigated the falling dynamics of wings with reduced models adapted from Kirchhoff's ordinary differential equations (ODEs) for the motion of bodies immersed in an irrotational flow. The non-dimensional momentum equations can be written as

$$I^\star \dot{v}_{x'} - (I^\star + 1)\dot{\theta} v_{y'} = -\Gamma v_{y'} - D_{x'} - \sin\theta, \tag{4.2a}$$

$$(I^\star + 1)\dot{v}_{y'} + I^\star \dot{\theta} v_{x'} = +\Gamma v_{x'} - D_{y'} - \cos\theta, \tag{4.2b}$$

where inertia and added mass appear on the left-hand side, while the right-hand side includes the lift force derived from the Kutta–Joukowski theorem, the drag force and gravity. Here, $v_{x'}$ and $v_{y'}$ are the components of the wing velocity $\boldsymbol{U}$ in the frame co-rotating with the wing (see figure 1*a*), $D_{x'}$ and $D_{y'}$ are the components of the drag force.

Previous studies rely crucially on empirical quasi-steady expressions for the wing circulation as a function of the instantaneous wing motion $v_{x'}$, $v_{y'}$ and $\dot{\theta}$ (Belmonte *et al.* 1998; Andersen *et al.* 2005). In contrast, we have deduced from our experiments that the lift force during gliding only depends on the circulation level generated at the turning point and that it remains constant throughout the gliding motion. Since no elastic deformations occur during gliding intervals, the dynamics of rigid and flexible wings can be modelled by (4.2) assuming a constant wing circulation (Mahadevan 1996), given by (4.1). Assuming that Γ remains constant simplifies (4.2) and allows the derivation of theoretical scalings for the flight characteristics. We note that by assuming a constant Γ, the shedding of the wake vortex Γ_{wake} and subsequent jump in wing circulation from Γ to $-\Gamma$ at the turning point is not adequately represented. Equations (4.2) hence only model a single gliding interval, corresponding a wing started from rest and whose motion is prescribed by (4.2) with constant Γ.

Equations (4.2) can be written in terms of v_x and v_y, the horizontal and vertical components of $\boldsymbol{U}$, and further simplified on the basis of experimental observations to derive theoretical scalings. We assume $I^\star \ll 1$, the pitch angle $\theta \ll 1$ during the gliding segments, leading to the simplified system

$$I^\star \dot{v}_x = -\Gamma v_y - D_x, \tag{4.3a}$$

$$\dot{v}_y = +\Gamma v_x - D_y - 1. \tag{4.3b}$$

Considering that the scale of the fluttering dynamics is determined by the inertia, added mass, lift and gravity terms in the coupled ODEs (4.3), we can directly deduce theoretical scalings for the different terms in the equations: the horizontal speed $v_x \sim 1/\Gamma$, the vertical descent speed $v_y \sim \sqrt{I^\star}/\Gamma$ and the time scale of the periodic motion $1/f \sim \sqrt{I^\star}/\Gamma$. Combination of these scalings yields scalings for the flight characteristics:

$$\Delta x \sim \frac{\sqrt{I^\star}}{\Gamma^2}, \quad \Delta y \sim \frac{I^\star}{\Gamma^2}, \quad f \sim \frac{\Gamma}{\sqrt{I^\star}}, \quad \tau_f \sim \frac{\Gamma}{\sqrt{I^\star}}. \tag{4.4a–d}$$

Equations (4.4) predict that the fluttering amplitudes Δx and Δy decrease with the wing circulation Γ squared and the frequency f and flight time τ_f linearly

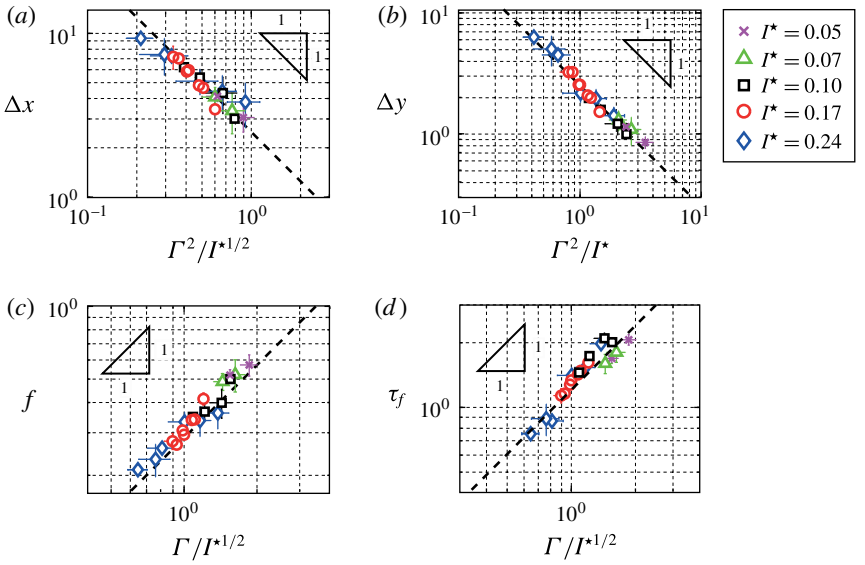

FIGURE 5. Comparison between experimental data recorded with high-speed imaging (symbols) and theoretical scalings (dashed line). Each data set corresponds to a given cross-sectional geometry. For each $I^\star$, the wing flexibility C_y is varied. The panels correspond to scalings for (*a*) Δx, the horizontal amplitude of the fluttering motion, (*b*) Δy, the vertical amplitude of the fluttering motion, (*c*) f, the frequency of the fluttering motion, (*d*) τ_f, the characteristic flight time. Scalings are expressed in terms of the wing circulation Γ and the added mass parameter $1/I^\star$. Here, Δx, Δy, f and τ_f are non-dimensional.

increase with Γ. From (4.4), the lift coefficient C_l can also be shown to be quadratic in Γ, $C_l \sim \Gamma^2$. These scalings are verified experimentally by plotting the non-dimensionalized flight characteristics measured from high-speed imaging as a function of the non-dimensional circulation measured from PIV experiments. Figure 5 presents experimental results on a 'log–log' scale for each separate wing geometry $I^\star$. For all four flight characteristics, the quadratic and linear scalings in Γ (4.4) are verified for each $I^\star$. The Cauchy number C_y does not directly appear in the scalings (4.4). However, as discussed previously, the circulation Γ depends on the flexibility since Γ–Γ_0 directly scales with $C_y^{3/2}$.

The theoretical scalings (4.4) depend on the wing dynamics through the non-dimensional moment of inertia $I^\star$, see (4.3). Taking into account the dependence on $I^\star$ allows for a full collapse of all the different experimental data sets with the theoretical scalings, requiring no fitting parameters. The full data collapse in figure 5 is in stark contrast to the data presented in figure 3, where the flight characteristics are presented as a function of the flexibility C_y. This collapse validates the physical picture described above. Combination of the theoretical analyses of the turning points and the gliding intervals fully rationalizes all experimental observations. For example, small passive elastic deformations of wings of $I^\star = 0.24$ occur at the turning points and lead to a more than twofold increase in Γ relative to their rigid counterparts, figure 4. This increase in circulation results in a more than twofold increase in flight time and fourfold increase in lift coefficient, see figure 5.

5. Conclusion

In summary, we have introduced a new model system to investigate the effect of flexibility on flight and lift generation. The present study establishes a positive and very substantial correlation between flexibility, wing circulation and lift generation, relevant to flapping flight. The extent of the lift increase is particularly striking: small bending deflections of 3–5 mm (no more than 5 % of the chord length) at the turning points result in an up to twofold increase in flight time and fourfold increase in lift coefficient C_l. Our study demonstrates the role of small passive elastic deformations at the origin of optimal lift increase. The formation of high wing circulation is directly related to the passive elastic acceleration of the trailing edge at the turning points. Theoretical scalings are derived in excellent agreement with experiments and identify the turning points as the crucial instants of unsteady lift generation. These theoretical scalings directly link the creation of additional circulation to elastic deformations (see figure 4). The detailed interactions between the flow and the deforming wing at the trailing edge have not been investigated and remain to be elucidated. Our results evidence the benefits of very small amplitude elastic deformations of the trailing edge in generating more lift, which could be advantageous to light biological systems. The Reynolds number $Re = 10^4$–10^5 and Cauchy number $C_y = 0$–100 in our study are relevant to many biological systems producing lift in the living world such as insects and winged seedpods. In this context, it is interesting to note that in these systems the chordwise bending stiffness can significantly decrease towards the trailing edge (Combes & Daniel 2003), leading to elastic deformations at the trailing edge.

The physics behind the lift enhancing mechanism rationalized in this study is fundamentally different from previously reported resonant mechanisms associated with thrust increase. The common view found in the literature is that propulsion can be enhanced by matching the flapping frequency to the resonance frequency of flexible wings, which in some cases may be energetically favourable (Alben 2008). In contrast, our study highlights the importance of very small deformations at turning points for lift increase. The lift enhancement mechanism identified in our study is non-resonant, and optimal lift generation is obtained far from resonance, the natural frequencies of the flexible wings ($\sim$10 Hz) being an order of magnitude higher than the fluttering frequency ($\sim$1 Hz).

This study also presents an ideal model system for the development and validation of aeroelastic modelling and computational approaches. The dynamics of our system includes all the relevant aspects of the flight dynamics of insects and MAVs: the dynamics of an entirely free body immersed in a fluid, aeroelasticity, unsteady aerodynamics, vortex generation and shedding. The scaling laws (4.4) are straightforward to verify. It is interesting to note that these scalings depend on both the Cauchy number C_y and the non-dimensional moment of inertia $I^\star$ and account for the elastic dynamics as well as the dynamics of freely falling wings. In particular, our theoretical scalings (4.4) and (4.1) are valid for fully rigid wings and predict the non-dimensional flight time to decrease with $\sqrt{I^\star}$. The validity of this scaling for rigid wings is verified by our experimental data (see figure 5). It is interesting to note that previously proposed approaches to model the aerodynamics of rigid fluttering wings fail to reproduce these scalings (Andersen *et al.* 2005). These studies use quasi-steady aerodynamics (Hu & Wang 2014) to model the aerodynamic forces as a function of the instantaneous angle of attack and linear and angular velocities of the wing and neglect the complex dynamics at the turning points. Our study suggests that the lift force during the gliding intervals is determined by how much circulation developed

around the wing at the previous turning point. Our simple theoretical model captures non-trivial aspects of the fluttering dynamics, which more intricate computational models do not, and highlights the necessity of accurately modelling the complex dynamics at the turning points in studies of unsteady falling plates.

Acknowledgements

The author is grateful to J. W. M. Bush for useful discussions throughout this work as well as M. Mercier and T. Peacock for their help in setting up the PIV experiments.

Supplementary movies

Supplementary movies are available at http://dx.doi.org/10.1017/jfm.2015.1.

References

ALBEN, S. 2008 Optimal flexibility of a flapping appendage in an inviscid fluid. *J. Fluid Mech.* **614**, 355–380.

ALBEN, S., SHELLEY, M. & ZHANG, J. 2002 Drag reduction through self-similar bending of a flexible body. *Nature* **420** (6915), 479–481.

ANDERSEN, A., PESAVENTO, U. & WANG, Z. 2005 Analysis of transitions between fluttering, tumbling and steady descent of falling cards. *J. Fluid Mech.* **541** (1), 91–104.

BELMONTE, A., EISENBERG, H. & MOSES, E. 1998 From flutter to tumble: inertial drag and Froude similarity in falling paper. *Phys. Rev. Lett.* **81**, 345–348.

BIRCH, J. M. & DICKINSON, M. H. 2001 Spanwise flow and the attachment of the leading-edge vortex on insect wings. *Nature* **412** (6848), 729–733.

COMBES, S. A. & DANIEL, T. L. 2003 Flexural stiffness in insect wings II. Spatial distribution and dynamic wing bending. *J. Expl. Biol.* **206** (17), 2989–2997.

ELOY, C., LAGRANGE, R., SOUILLIEZ, C. & SCHOUVEILER, L. 2008 Aeroelastic instability of cantilevered flexible plates in uniform flow. *J. Fluid Mech.* **611** (1), 97–106.

HEATHCOTE, S. & GURSUL, I. 2007 Flexible flapping airfoil propulsion at low Reynolds numbers. *AIAA J.* **45** (5), 1066–1079.

HEISINGER, L., NEWTON, P. & KANSO, E. 2014 Coins falling in water. *J. Fluid Mech.* **742**, 243–253.

HU, R. & WANG, L. 2014 Motion transitions of falling plates via quasisteady aerodynamics. *Phys. Rev.* E **90** (1), 013020.

HUANG, W., LIU, H., WANG, F., WU, J. & ZHANG, H. P. 2013 Experimetal study of a freely falling plate with an inhomogeneous mass distribution. *Phys. Rev.* E **88** (5), 053008.

MAHADEVAN, L. 1996 Tumbling of a falling card. *C. R. Acad. Sci. Paris II* **323**, 729–736.

MASOUD, H. & ALEXANDER, A. 2010 Resonance of flexible flapping wings at low Reynolds number. *Phys. Rev.* E **81** (5), 056304.

MICHELIN, S. & LLEWELLYN-SMITH, S. G. 2009 Resonance and propulsion performance of a heaving flexible wing. *Phys. Fluids* **21**, 071902.

PERCIN, M., HU, Y., VAN OUDHEUSDEN, B. W., REMES, B. & SCARANO, F. 2011 Wing flexibility effects in clap-and-fling. *Intl J. Micro Air Veh.* **3** (4), 217–227.

RAMANANARIVO, S., GODOY-DIANA, R. & THIRIA, B. 2011 Rather than resonance, flapping wing flyers may play on aerodynamics to improve performance. *Proc. Natl Acad. Sci.* **108** (15), 5964–5969.

SHELLEY, M., VANDENBERGHE, N. & ZHANG, J. 2005 Heavy flags undergo spontaneous oscillations in flowing water. *Phys. Rev. Lett.* **94** (9), 094302.

SPAGNOLIE, S. E., MORET, L., SHELLEY, M. J. & ZHANG, J. 2010 Surprising behaviors in flapping locomotion with passive pitching. *Phys. Fluids* **22** (4), 041903.

TAM, D., BUSH, J. W. M., ROBITAILLE, M. & KUDROLLI, A. 2010 Tumbling dynamics of passive flexible wings. *Phys. Rev. Lett.* **104** (18), 184504.

TCHOUFAG, J., FABRE, D. & MAGNAUDET, J. 2014 Global linear stability analysis of the wake and path of buoyancy-driven disks and thin cylinders. *J. Fluid Mech.* **740**, 278–3111.

ZHAO, L., HUANG, Q., DENG, X. & SANE, S. P. 2010 Aerodynamic effects of flexibility in flapping wings. *J. R. Soc. Interface* **7** (44), 485–497.